# Voltage Stability Constrained Optimal Power Flow for Unbalanced Distribution System Based on Semidefinite Programming

Yanling Lin, *Student Member*, *IEEE*, Xiaohu Zhang, *Senior Member*, *IEEE*, Jianhui Wang, *Fellow*, *IEEE*, Di Shi, *Senior Member*, *IEEE*, and Desong Bian, *Member*, *IEEE*

***Abstract*—This paper proposes a voltage stability constrained optimal power flow (VSC-OPF) for an unbalanced distribution system with distributed generators (DGs) based on semidefinite programming (SDP). The AC optimal power flow (ACOPF) for unbalanced distribution systems is formulated as a chordal relaxation-based SDP model. The minimal singular value (MSV) of the power flow Jacobian matrix is adopted to indicate the voltage stability margin. The Jacobian matrix can be explicitly expressed by ACOPF state variables. The nonlinear constraint on the Jacobian MSV is then replaced with its maximal convex subset using linear matrix inequality (LMI), which can be incorporated in the SDP-based ACOPF formulation. A penalty technique is leveraged to improve the exactness of the SDP relaxation. Case studies performed on several IEEE test systems validate the effectiveness of the proposed method.**

***Index Terms*—Voltage stability, semidefinite programming, Jacobian matrix, optimal power flow.**

## I. Introduction

POWER systems are the backbone of our economy. Nowadays, the increasing load and stochastic disturbances from renewable energy have driven some systems to operate near their limit, including the voltage stability margin (VSM) [1]-[3]. Voltage stability refers to the ability of power system to sustain steady acceptable voltages at all buses under normal operating conditions and possible external disturbances [4]. Traditionally, optimal power flow (OPF) models enforce security constraints such as voltage magnitude limits and line flow limits. Nevertheless, it is insufficient to guarantee the secured operation in modern power systems by only enforcing the thermal and voltage magnitude limits [5]. By including constraints on voltage stability, voltage stability constrained OPF (VSC-OPF) models can ensure steady-state voltage stability and maintain a sufficient loading margin. Owing to these benefits, there is a growing interest in VSC-OPF.

VSC-OPF involves the constraints on voltage stability index (VSI). One way to define the VSI is to use the proportional increase of load. To formulate a VSC-OPF model, the model in [6] defines the maximum loading value as an index to measure the distance of a system to collapse and incorporate that into an OPF problem. In [7], OPF is performed to ensure that the operating point exists at the desired load level given a VSM. In [8], voltage stability is considered in a wind power planning problem. To enhance the steady-state stability of smart distribution system, [9] suggests a multi-timescale voltage stability constrained volt/var optimization model. Support from the natural gas subsystem in an energy hub is shown to help maintain the voltage stability in the power system [10]. Despite wide application of load margin, with this VSI, only one direction of load variation is considered for the load margin.

Based on the equivalent model of a two-bus system, the maximum loadability of a line can be calculated, which leads to many heuristic VSIs [11]. Reference [12] enhances the distribution system voltage stability by reconfiguration. A VSI is proposed in [13], and its ability to detest the onset of voltage instability is verified. Reference [14] proposes a line-wise power flow formulation and the corresponding voltage collapse index, and [15] integrates the index in the optimal power flow. The L-index is adopted in a microgrid unit commitment problem in [16]. These indices are local indices, which can help identify critical lines and buses, but are not directly connected to a global VSM.

Previous studies have found that the collapse point of the voltage can be correlated with the saddle-node bifurcation or limit induced bifurcation; in each case, at the collapse point, the power flow Jacobian matrix is either singular or close to singular [6]. Thus the steady-state voltage stability can be evaluated by analyzing the singularity of the power flow Jacobian matrix. The power flow Jacobian matrix is the linearized relationship between power injection and voltage deviation. As the matrix becomes singular, a small load change will lead to a substantial voltage change and instability [17].

Manuscript received: April 4, 2021; revised: July 27, 2021; accepted: February 8, 2022. Date of CrossCheck: February 8, 2022. Date of online publication: April 29, 2022.

This work was funded by State Grid Corporation of China (SGCC) under project "Hybrid Energy Storage Management Platform for Integrated Energy System" (No. SGGR0000DLJS1800932).



Y. Lin, X. Zhang (corresponding author), D. Shi, and D. Bian are with GEIRI North America, San Jose, USA, and Y. Lin is also with Southern Methodist University, Dallas, USA (e-mail: yanlingl@mail.smu.edu; youwen9h@gmail.com; di.shi@asu.edu; biandesong@gmail.com).

J. Wang is with Southern Methodist University, Dallas, USA (e-mail: jianhui@mail.smu.edu).

DOI: 10.35833/MPCE.2021.000220

In [18], an index based on a sufficient condition for the non-singularity of power flow Jacobian matrix is proposed to represent the distance between the operating point to the solvability boundary. Reference [5] further extends the work in [18] and proposes a second-order conic representation of the condition and incorporate it into the OPF model of a transmission system. On the basis of the widely-adopted branch flow OPF model, [19] proposes the determinant of the Jacobian matrix as a VSI.

The minimum singular value (MSV) of the power flow Jacobian matrix indicates its closeness to singularity [20]. Therefore, [17] and [21] use the MSV of power flow Jacobian matrix as an index for voltage stability assessment. The MSV threshold is incorporated as a constraint to ensure static voltage stability in [22]-[24]. Reference [1] addresses the issues of non-explicit and non-convex of MSV constraints and formulates the MSV constraint as an SDP constraint. A computationally tractable iterative linear programming solution using singular value sensitivities is proposed in [25]. In summary, MSV is an implicit function of the optimization variables, and the integration of MSV constraint remains a challenge for OPF.

The voltage stability can be analyzed by the steady-state OPF disregarding the system dynamics because the long-term voltage stability problem is essentially loadability problem. In contrary, the transient stability deals with the short-term stability issues of contingency, and transient-stability constrained OPF (TSC-OPF) is a nonlinear optimization problem with differential-algebraic equation (DAE) constraints [26]. Previous research efforts focus on dealing with differential equations in the TSC-OPF through numerical optimization methods, including discretization [27] and integration of time-domain simulation in OPF [28]. Another branch of TSC-OPF drops the DAE, and TSC-OPF problems are reduced to nonlinear OPF with a transient stability constraint, similar to the formulation of VSC-OPF. Then the meta-heuristic optimization methods can be used to solve the dynamic stability constrained problems [29], [30] and steady voltage stability constrained problems [31]. Reference [32] takes one step further and presents an OPF framework that can simultaneously consider the dynamic and steady-state voltage stabilities. Aiming to approximate the nonlinear relationship between state variables and voltage stability margin, [33], [34] and [35], [36] report progress using neural network to estimate transient stability and steady-state stability margin, respectively. The above works illustrate that the TSC-OPF and VSC-OPF are both nonlinear optimization problems and can benefit from the research breakthroughs of each other.

While traditionally, voltage stability analysis is carried out for transmission systems, recent research works recognize that voltage stability issues exist in the distribution system [18] or even microgrids [16]. According to [18], the ability to assess and maintain the security margins within the operational context of growing deployment of distributed generators (DGs) is essential to modernized power distribution systems. The integration of DGs further complicates the problems of power flow solvability and voltage stability. According to [7], the voltage instability of distribution systems can spread to the corresponding transmission grid. In [37] and [38], voltage stability is improved from DG planning. The method in [18] is also extended to the microgrid level in [39]. VSC-OPF is carried out for different topics such as real-time voltage stability assessment [40], reconfiguration [12], wind power integration [13], and DG installation [19]. These works demonstrate that the distribution system awaits more efforts on VSC-OPF investigation.

Another limitation of the existing works is that most of the VSC-OPF methods deal with the single-phase system models. Concerning three-phase unbalanced systems, a voltage stability analysis method based on the continuation power flow method is proposed in [3]. Reference [41] presents a nonlinear OPF method for the unbalanced transmission system, which maximizes the load demand at a specified bus, and this maximum loading point is regarded as the VSM. The maximum loading point is extended in [42] to a multi-stage and probabilistic framework. The works mentioned above show that the approximation of unbalanced system with its single-phase equivalent provides unreliable voltage stability assessment results. Furthermore, none of the existing works addresses the economic operation of power system while maintaining the VSM above a given threshold at the same time.

Based on these observations, the contributions of this paper can be summarized as follows.

1) A VSC-OPF framework is proposed for the unbalanced distribution power system with DGs. The AC power flow of the unbalanced distribution system is formulated as a chordal relaxation-based SDP model; and the proposed method can be incorporated into the daily economic dispatch of the distribution system.

2) In the VSC-OPF, the voltage stability constraint is enforced through the MSV of the power flow Jacobian matrix. The MSV is expressed explicitly by the state variables of the OPF. The nonlinear constraint on power flow MSV is replaced by a linear matrix inequality constraint (LMI), and the LMI constraint can be easily incorporated in the convexified OPF formulation.

3) A penalty technique is leveraged to improve the exactness of the SDP relaxation.

4) The proposed multi-period operation framework and case studies thoroughly exemplify the contribution of energy storage system (ESS).

The rest of the paper is organized as follows. Section II gives the SDP-based ACOPF formulation. Section III details the SDP-based VSC-OPF formulation. Simulation results are provided in Section IV. Finally, conclusions are drawn in Section V.

## II. SDP-BASED ACOPF FORMULATION

In this section, the SDP models are derived for an unbalanced distribution system. For the SDP-based ACOPF formulation, we leverage the bus injection model (BIM) provided in [43]. We will use the ACOPF state variables to explicitly express the power flow Jacobian matrix.

### A. ACOPF Model for Unbalanced Distribution System

In a distribution system, we use $\mathcal{N}=\{1,2,\ldots,n+1\}$ to denote the set of buses. The system contains a single substation connected to the upstream system that acts as the slack bus. Without the loss of generality, we number the buses so that the set of PQ bus is $\{1,2,...,m\}$, the set of PV bus is $\{m+1,m+2,...,n\}$, and the $(n+1)^{\text{th}}$ bus is the slack bus.

In this subsection, we will first introduce the BIM for an unbalanced system. Let $\boldsymbol{\Phi}_i$ be the set of phases of bus $i$, and $\boldsymbol{\Phi}_{ij}$ be the phases of the line $i\to j$. The ordered pair $(i,j)\in E$ denotes the set of lines, and we assume that their direction $i\to j$ follows $\boldsymbol{\Phi}_j=\boldsymbol{\Phi}_{ij}\subseteq\boldsymbol{\Phi}_i$. For example, if a double-phase line $(i,j)$ connects a three-phase bus and double-phase bus, then we will number the buses so that $\boldsymbol{\Phi}_i=\{a,b,c\}$, $\boldsymbol{\Phi}_{ij}=\boldsymbol{\Phi}_j=\{b,c\}$. We use $i\sim j$ to denote either $i\to j$ or $j\to i$. $\boldsymbol{V}_i\in\mathbb{C}^{|\boldsymbol{\Phi}_i|}$ is the complex voltage vector of bus $i$. $\boldsymbol{z}_{ij}\in\mathbb{C}^{|\boldsymbol{\Phi}_{ij}|\times|\boldsymbol{\Phi}_{ij}|}$ is the line impedance of $(i,j)$, and the line admittance $\boldsymbol{y}_{ij}=\boldsymbol{z}_{ij}^{-1}$. Let $\boldsymbol{Y}$ be the system admittance matrix, and $\boldsymbol{Y}_{ij}$ indicates the sub-matrix corresponding to buses $i$ and $j$, which has components $Y_{ij}^{\varphi\phi}=G_{ij}^{\varphi\phi}+\mathrm{j}B_{ij}^{\varphi\phi}$.

The complex power injection to bus $i$ will be:

$$\boldsymbol{p}_{i,t}+\mathrm{j}\boldsymbol{q}_{i,t}=\sum_{j\in\mathcal{N}}\mathrm{diag}\left\{\boldsymbol{V}_i^{\boldsymbol{\Phi}_{ij}}(\boldsymbol{Y}_{ij}\boldsymbol{V}_j^{\boldsymbol{\Phi}_{ij}})^H\right\}\quad i\in\mathcal{N}\tag{1}$$

where the superscript $H$ indicates the Hermitian conjugate.

Concerning power sources, the distribution system is supplied by the upstream network, and within it there are DGs and ESSs. Let $p_g^\varphi$ and $q_g^\varphi$ be the active power and reactive power provided by DGs at bus $i$ of phase $\varphi\in\boldsymbol{\Phi}_i$, respectively. Similarly, we can define $p_b^\varphi+\mathrm{j}q_b^\varphi$ for the active power and reactive power from the upstream network. The discharging active power and charging active power from the ESSs are $dis_s^\varphi$ and $ch_s^\varphi$, respectively; and ESSs can also provide reactive power $\mathrm{j}q_s^\varphi$.

In the daily operation, the objective is to minimize the operation costs of distribution system within the prediction horizon. Rolling-horizon optimization is employed to make optimal operation decisions, which is illustrated in Fig. 1. The optimization is performed for the look-ahead window, but only the first interval results are preserved. The above process is repeated for the whole day. We assume perfect predictions for the locational marginal price (LMP), load, and renewable output for the look-ahead window, and therefore, the proposed OPF is a deterministic optimization problem.

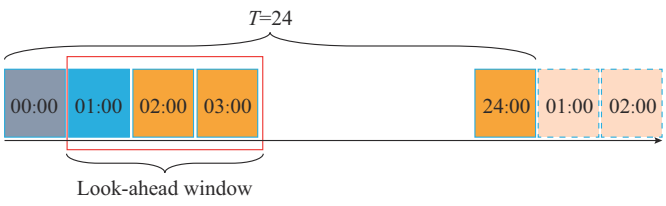


Fig. 1. Illustration of rolling-horizon optimization.

Equations (2)-(23) give the complete ACOPF formulation.

$$\min\sum_{t=t_0}^{t_0+T_p}\left[p_{b,t}c_{b,t}+\sum_{g\in\mathcal{G}}p_{g,t}c_g+\sum_{s\in\mathcal{S}}(ch_{s,t}+dis_{s,t})c_s\right]\Delta t\tag{2}$$

s.t.

$$p_{i,t}^\varphi=\sum_{j\in\mathcal{N}}\sum_{\phi\in\boldsymbol{\Phi}_{ij}}(G_{ij}^{\varphi\phi}\Re(V_{i,t}^\varphi V_{j,t}^{\phi*})+B_{ij}^{\varphi\phi}\Im(V_{i,t}^\varphi V_{j,t}^{\phi*}))\tag{3}$$

$$q_{i,t}^\varphi=\sum_{j\in\mathcal{N}}\sum_{\phi\in\boldsymbol{\Phi}_{ij}}(-B_{ij}^{\varphi\phi}\Re(V_{i,t}^\varphi V_{j,t}^{\phi*})+G_{ij}^{\varphi\phi}\Im(V_{i,t}^\varphi V_{j,t}^{\phi*}))\tag{4}$$

$$V_i^{\min}\le V_{i,t}^\varphi\le V_i^{\max}\quad\forall i,\forall\varphi,\forall t\tag{5}$$

$$S_{ij}^{\min}\le\left|\mathrm{diag}\left\{\boldsymbol{V}_{i,t}^{\boldsymbol{\Phi}_{ij}}\left[\boldsymbol{Y}_{ij}(\boldsymbol{V}_{i,t}^{\boldsymbol{\Phi}_{ij}}-\boldsymbol{V}_{j,t})\right]^H\right\}\right|\le S_{ij}^{\max}\quad\forall i\sim j,\forall t\tag{6}$$

$$p_{i,t}^\varphi=\sum_{b\in\mathcal{U}_i}p_{b,t}^\varphi+\sum_{g\in\mathcal{G}_i}p_{g,t}^\varphi+\sum_{s\in\mathcal{S}_i}(dis_{s,t}^\varphi-ch_{s,t}^\varphi)-pd_{i,t}^\varphi\tag{7}$$

$$q_{i,t}^\varphi=\sum_{b\in\mathcal{U}_i}q_{b,t}^\varphi+\sum_{g\in\mathcal{G}_i}q_{g,t}^\varphi+\sum_{s\in\mathcal{S}_i}q_{s,t}^\varphi-qd_{i,t}^\varphi\tag{8}$$

$$p_{b,t}=\sum_{\varphi\in\boldsymbol{\Phi}_b}p_{b,t}^\varphi\tag{9}$$

$$p_{g,t}=\sum_{\varphi\in\boldsymbol{\Phi}_g}p_{g,t}^\varphi\tag{10}$$

$$q_{b,t}=\sum_{\varphi\in\boldsymbol{\Phi}_b}q_{b,t}^\varphi\tag{11}$$

$$q_{g,t}=\sum_{\varphi\in\boldsymbol{\Phi}_g}q_{g,t}^\varphi\tag{12}$$

$$p_{g,t}^{\min}\le p_{g,t}\le p_{g,t}^{\max}\tag{13}$$

$$q_{g,t}^{\min}\le q_{g,t}\le q_{g,t}^{\max}\tag{14}$$

$$ch_{s,t}=\sum_{\varphi\in\boldsymbol{\Phi}_s}ch_{s,t}^\varphi\tag{15}$$

$$dis_{s,t}=\sum_{\varphi\in\boldsymbol{\Phi}_s}dis_{s,t}^\varphi\tag{16}$$

$$q_{s,t}=\sum_{\varphi\in\boldsymbol{\Phi}_s}q_{s,t}^\varphi\tag{17}$$

$$SOC_{s,t}-(1-\alpha_s)SOC_{s,t-1}=(ch_{s,t}\cdot\eta_s-dis_{s,t}/\eta_s)\Delta t\tag{18}$$

$$SOC_s^{\min}\le SOC_{s,t}\le SOC_s^{\max}\tag{19}$$

$$ch_s^{\min}\le ch_{s,t}\le ch_s^{\max}\tag{20}$$

$$dis_s^{\min}\le dis_{s,t}\le dis_s^{\max}\tag{21}$$

$$(dis_{s,t}-ch_{s,t})^2+q_{s,t}^2\le dis_s^{\max}\tag{22}$$

$$\sigma_{\min}(\boldsymbol{J}_{PF,t_0})\ge\sigma_{ref}\tag{23}$$

where $t_0$ and $T_p$ are the starting time and look-ahead window, respectively; $c_{b,t}$, $c_g$, and $c_s$ are the linear prices for buying power from the upstream system, DG output, and ESS charging/discharging, respectively; $pd_{i,t}^\varphi$ and $qd_{i,t}^\varphi$ are the nodal active and reactive loads, respectively; $\Re(x)$ and $\Im(x)$ are the real and imaginary parts of the complex number $x$, respectively; $p_{i,t}^\varphi$ and $q_{i,t}^\varphi$ are the elements in power injection vector $\boldsymbol{p}_{i,t}$ and $\boldsymbol{q}_{i,t}$, respectively; $\mathcal{U}_i$, $\mathcal{G}_i$, and $\mathcal{S}_i$ are the sets of the upstream system connection point, DGs, and ESSs at node $i$, respectively, and can be an empty set if they do not exist; $V_i^{\min}$, $V_i^{\max}$, $S_{ij}^{\min}$, $S_{ij}^{\max}$ are the lower and upper limits of voltage and line flow, respectively; $p_{g,t}^{\min}$, $p_{g,t}^{\max}$, $q_{g,t}^{\min}$, $q_{g,t}^{\max}$ are the the lower and upper limits of active and reactive power of DGs, respectively; $\eta_s$ is the charging/discharging ef-

ficiency coefficient; *SOC* is the state of charge variable; $\alpha_s$ is the energy storage self-discharging ratio; $ch_s^{\min}$, $ch_s^{\max}$, $dis_s^{\min}$, $dis_s^{\max}$ are the lower and upper limits of charging and discharging power, respectively; $\sigma_{\min}(\boldsymbol{J}_{PF,t_0})$ is the MSV of the power flow Jacobian matrix $\boldsymbol{J}_{PF}$; and $\sigma_{ref}$ is the given voltage stability margin. Equations (3) and (4) are the power injection constraints that indicate the nodal power balance; (5) and (6) are the constraints for voltage amplitude and line capacity, respectively; (9)-(14) are the constraints on power output from power resources; and (15)-(19) are the constraints on ESS.

It should be noted that the ESSs can provide reactive power support to the distribution system. Variables on the left side in (9)-(12) and (15)-(17) represent the summation of the variables on the right side over all the possible phases, e.g., $p_{b,t}$ is the total active power injection from the upstream network over phases $\{a,b,c\}$.

In this paper, we treat the MSV of $\boldsymbol{J}_{PF}$ as a signal of voltage stability, that is, we would operate the power system with a pre-defined VSM, which gives rise to (23). Concretely, (23) constrains the MSV of $\boldsymbol{J}_{PF}$ above $\sigma_{ref}$. In the rolling-horizon scheme, only the result of the first interval will be used. We thus only enforce (23) in the first interval to decrease the computation burden.

### *B. SDP-based ACOPF Relaxation*

The nonlinear constraints (3) and (4) can be convexified by SDP formulation. The standard SDP relaxation introduces a symmetric matrix $\boldsymbol{W}$ [43]:

$$\boldsymbol{W}=\begin{bmatrix}\boldsymbol{V}_1\\ \boldsymbol{V}_2\\ \vdots\\ \boldsymbol{V}_{n+1}\end{bmatrix}\begin{bmatrix}\boldsymbol{V}_1^H & \boldsymbol{V}_2^H & \cdots & \boldsymbol{V}_{n+1}^H\end{bmatrix} \tag{24}$$

Shift the nonconvexity from (1) to $\boldsymbol{W}\succcurlyeq 0$, $rank(\boldsymbol{W})=1$, and then remove the rank constraint. Notice that only blocks corresponding to lines $(i,j)$ appear in other constraints besides $\boldsymbol{W}\succcurlyeq 0$. We can perform chordal relaxation by only defining the blocks $\boldsymbol{W}_{ij}$ in $\boldsymbol{W}$ that corresponds to real lines in the system:

$$\boldsymbol{W}_{ij}=\begin{bmatrix}\boldsymbol{u}_i^{\Phi_{ij}} & \boldsymbol{X}_{ij}\\ \boldsymbol{X}_{ji} & \boldsymbol{u}_j\end{bmatrix}=\begin{bmatrix}\boldsymbol{V}_i^{\Phi_{ij}}\\ \boldsymbol{V}_j\end{bmatrix}\begin{bmatrix}\boldsymbol{V}_i^{\Phi_{ij}}\\ \boldsymbol{V}_j\end{bmatrix}^H \quad (i,j)\in E \tag{25}$$

where $\boldsymbol{u}_i\in\mathbb{C}^{|\Phi_i|\times|\Phi_i|}$; and $\boldsymbol{X}_{ij}\in\mathbb{C}^{|\Phi_{ij}|\times|\Phi_{ij}|}$. It should be noted that $\boldsymbol{X}_{ji}=\boldsymbol{X}_{ij}^H$, $\forall(i,j)\in E$; and $\begin{bmatrix}\boldsymbol{u}_i^{\Phi_{ij}} & \boldsymbol{X}_{ij}\\ \boldsymbol{X}_{ji} & \boldsymbol{u}_j\end{bmatrix}\succcurlyeq 0$ is rank one, $\forall(i,j)\in E$.

It is common practice to replace $\boldsymbol{W}\succcurlyeq 0$ with $\begin{bmatrix}\boldsymbol{u}_i^{\Phi_{ij}} & \boldsymbol{X}_{ij}\\ \boldsymbol{X}_{ji} & \boldsymbol{u}_j\end{bmatrix}\succcurlyeq 0$, $\forall(i,j)$ to exploit the radial network topology to reduce computation burden [43], [44]. For unbalanced distribution systems with a radial network, the graphs of their OPF problems are chordal, and the above replacement is based on chordal relaxation. For the meshed networks whose graphs are no longer chordal, this replacement can be interpreted as requiring the principal submatrices of $\boldsymbol{W}$ to be positive semi-definite, which is the necessary condition for $\boldsymbol{W}\succcurlyeq 0$ [45]. Therefore, our formulation is also applicable to the meshed networks, but replacing $\boldsymbol{W}\succcurlyeq 0$ with its necessary conditions might be less numerically tractable.

We can now replace the elements of complex voltage vectors in (3) and (4) by elements in $\boldsymbol{W}_{ij}$. We further define dummy variables $c_{ij}^{\varphi\phi}$ and $s_{ij}^{\varphi\phi}$ for the real and reactive parts of matrix $\boldsymbol{W}_{ij}$.

$$c_{ii}^{\varphi\phi}=\Re(V_i^{\varphi}V_i^{\phi})=\Re(u_i^{\varphi\phi}) \tag{26}$$

$$s_{ii}^{\varphi\phi}=-\Im(V_i^{\varphi}V_i^{\phi})=-\Im(u_i^{\varphi\phi}) \tag{27}$$

$$c_{ij}^{\varphi\phi}=\Re(V_i^{\varphi}V_j^{\phi})=\Re(X_{ij}^{\varphi\phi}) \tag{28}$$

$$s_{ij}^{\varphi\phi}=-\Im(V_i^{\varphi}V_j^{\phi})=-\Im(X_{ij}^{\varphi\phi}) \tag{29}$$

$$\begin{cases}c_{ji}^{\phi\varphi}=c_{ij}^{\varphi\phi}\\ s_{ji}^{\phi\varphi}=-s_{ij}^{\varphi\phi}\end{cases} \tag{30}$$

$$\begin{cases}c_{ji}^{\phi\varphi}=c_{ij}^{\varphi\phi}\\ s_{ji}^{\phi\varphi}=-s_{ij}^{\varphi\phi}\end{cases} \tag{31}$$

It should also be noted that $s_{ii}^{\varphi\varphi}=0$. Now we can reformulate the power flow constraints using $s$ and $c$. The complete formulation of the SDP-based ACOPF is described by the objective (2) with (7)-(22) and the following constraints.

$$p_i^{\varphi}=\sum_{\phi\in\Phi_i}(c_{ii}^{\varphi\phi}G_{ii}^{\varphi\phi}-s_{ii}^{\varphi\phi}B_{ii}^{\varphi\phi})+\sum_{j:i\sim j}\sum_{\phi\in\Phi_{ij}}(c_{ij}^{\varphi\phi}G_{ij}^{\varphi\phi}-s_{ii}^{\varphi\phi}B_{ij}^{\varphi\phi}) \tag{32}$$

$$q_i^{\varphi}=\sum_{\phi\in\Phi_i}(-c_{ii}^{\varphi\phi}B_{ii}^{\varphi\phi}-s_{ii}^{\varphi\phi}G_{ii}^{\varphi\phi})+\sum_{j:i\sim j}\sum_{\phi\in\Phi_{ij}}(-c_{ij}^{\varphi\phi}B_{ij}^{\varphi\phi}-s_{ii}^{\varphi\phi}G_{ij}^{\varphi\phi}) \tag{33}$$

$$(V_i^{\min})^2\le c_{ii,t}^{\varphi\varphi}\le(V_i^{\max})^2\quad\forall i,\forall\varphi,\forall t \tag{34}$$

$$S_{ij}^{\min}\le\left|\operatorname{diag}\left\{(\boldsymbol{u}_{i,t}^{\Phi_{ij}}-\boldsymbol{X}_{ij,t})\boldsymbol{Y}_{ij}^H\right\}\right|\le S_{ij}^{\max}\quad\forall i\sim j,\forall t \tag{35}$$

$$\begin{bmatrix}\boldsymbol{u}_i^{\Phi_{ij}} & \boldsymbol{X}_{ij}\\ \boldsymbol{X}_{ij}^H & \boldsymbol{u}_j\end{bmatrix}\succcurlyeq 0\quad\forall(i,j)\in E \tag{36}$$

The above SDP-based ACOPF formulation is convex except for constraint (23). To convexify this constraint, we need to first obtain an explicit formulation of $\boldsymbol{J}_{PF}$ using state variables $s$ and $c$, which will be introduced in the next subsection.

### *C. $\boldsymbol{J}_{PF}$ for Unbalanced System*

The power flow Jacobian matrix of the unbalanced system is used to study the voltage stability level of the distribution system, which can be expressed in (37), where the sub-matrix $\boldsymbol{J}_{xy}$ $(x=P,Q,\ y=\theta,V)$ corresponds to $x$ on the left vector and $y$ on the right vector.

$$\begin{bmatrix}\Delta p_1^{\varphi}\\ \Delta p_2^{\varphi}\\ \vdots\\ \Delta p_n^{\phi}\\ \Delta q_1^{\varphi}\\ \Delta q_2^{\varphi}\\ \vdots\\ \Delta q_m^{\phi}\end{bmatrix}=\begin{bmatrix}\boldsymbol{J}_{P\theta} & \boldsymbol{J}_{PV}\\ \boldsymbol{J}_{Q\theta} & \boldsymbol{J}_{QV}\end{bmatrix}\begin{bmatrix}\Delta\theta_1^{\varphi}\\ \Delta\theta_2^{\varphi}\\ \vdots\\ \Delta\theta_n^{\phi}\\ \Delta|V_1^{\varphi}|/|V_1^{\varphi}|\\ \Delta|V_2^{\varphi}|/|V_2^{\varphi}|\\ \vdots\\ \Delta|V_m^{\phi}|/|V_m^{\phi}|\end{bmatrix} \tag{37}$$

The elements of Jacobian matrix are obtained by taking

derivatives of the nodal power injection over voltage angle $\theta$ and amplitude $|V|$. Note that we introduce $c$ and $s$ to represent power injection in (32) and (33), respectively, and the relationships can be derived as:

$$\begin{cases} \dfrac{\partial c_{ij}^{\varphi\phi}}{\partial \theta_j^{\phi}} = -s_{ij}^{\varphi\phi} \\ \dfrac{\partial s_{ij}^{\varphi\phi}}{\partial \theta_j^{\phi}} = c_{ij}^{\varphi\phi} \end{cases} \tag{38}$$

$$\begin{cases} \dfrac{\partial c_{ij}^{\varphi\phi}}{\partial \theta_i^{\varphi}} = s_{ij}^{\varphi\phi} \\ \dfrac{\partial s_{ij}^{\varphi\phi}}{\partial \theta_i^{\varphi}} = -c_{ij}^{\varphi\phi} \end{cases} \tag{39}$$

Thus, the Jacobian matrix can be explicitly formulated in terms of the state variables.

The elements in the Jacobian matrix are categorized into different categories.

*1) Off Diagonal Elements for $i \neq j$*

$$\frac{\partial \Delta P_i^{\varphi}}{\partial \theta_j^{\phi}} = G_{ij}^{\varphi\phi} s_{ij}^{\varphi\phi} + B_{ij}^{\varphi\phi} c_{ij}^{\varphi\phi} \tag{40}$$

$$\frac{\partial \Delta P_i^{\varphi}}{\partial |V_j^{\phi}|} |V_j^{\phi}| = -G_{ij}^{\varphi\phi} c_{ij}^{\varphi\phi} + B_{ij}^{\varphi\phi} s_{ij}^{\varphi\phi} \tag{41}$$

$$\frac{\partial \Delta Q_i^{\varphi}}{\partial \theta_j^{\phi}} = G_{ij}^{\varphi\phi} c_{ij}^{\varphi\phi} - B_{ij}^{\varphi\phi} s_{ij}^{\varphi\phi} \tag{42}$$

$$\frac{\partial \Delta Q_i^{\varphi}}{\partial |V_j^{\phi}|} |V_j^{\phi}| = G_{ij}^{\varphi\phi} s_{ij}^{\varphi\phi} + B_{ij}^{\varphi\phi} c_{ij}^{\varphi\phi} \tag{43}$$

*2) Off Diagonal Elements for $i = j, \varphi \neq \phi$*

$$\frac{\partial \Delta P_i^{\varphi}}{\partial \theta_i^{\phi}} = G_{ii}^{\varphi\phi} s_{ii}^{\varphi\phi} + B_{ii}^{\varphi\phi} c_{ii}^{\varphi\phi} \tag{44}$$

$$\frac{\partial \Delta P_i^{\varphi}}{\partial |V_i^{\phi}|} |V_i^{\phi}| = -G_{ii}^{\varphi\phi} c_{ii}^{\varphi\phi} + B_{ii}^{\varphi\phi} s_{ii}^{\varphi\phi} \tag{45}$$

$$\frac{\partial \Delta Q_i^{\varphi}}{\partial \theta_i^{\phi}} = G_{ii}^{\varphi\phi} c_{ii}^{\varphi\phi} - B_{ii}^{\varphi\phi} s_{ii}^{\varphi\phi} \tag{46}$$

$$\frac{\partial \Delta Q_i^{\varphi}}{\partial |V_i^{\phi}|} |V_i^{\phi}| = G_{ii}^{\varphi\phi} s_{ii}^{\varphi\phi} + B_{ii}^{\varphi\phi} c_{ii}^{\varphi\phi} \tag{47}$$

*3) Diagonal Elements*

$$\frac{\partial \Delta P_i^{\varphi}}{\partial \theta_i^{\varphi}} = \sum_{\phi \neq \varphi} \left( -G_{ii}^{\varphi\phi} s_{ii}^{\varphi\phi} - B_{ii}^{\varphi\phi} c_{ii}^{\varphi\phi} \right) - \sum_{j:i\sim j} \sum_{\phi \in \Phi_{ij}} \left( G_{ij}^{\varphi\phi} s_{ij}^{\varphi\phi} + B_{ij}^{\varphi\phi} c_{ij}^{\varphi\phi} \right) = q_{i,t}^{\varphi} + B_{ii}^{\varphi\varphi} c_{ii}^{\varphi\varphi} \tag{48}$$

$$\frac{\partial \Delta P_i^{\varphi}}{\partial |V_i^{\varphi}|} |V_i^{\varphi}| = -2G_{ii}^{\varphi\varphi} c_{ii}^{\varphi\varphi} + \sum_{\phi \neq \varphi} \left( -G_{ii}^{\varphi\phi} c_{ii}^{\varphi\phi} + B_{ii}^{\varphi\phi} s_{ii}^{\varphi\phi} \right) + \sum_{j:i\sim j} \sum_{\phi \in \Phi_{ij}} \left( -G_{ij}^{\varphi\phi} c_{ij}^{\varphi\phi} + B_{ij}^{\varphi\phi} s_{ij}^{\varphi\phi} \right) = -p_{i,t}^{\varphi} - G_{ii}^{\varphi\varphi} c_{ii}^{\varphi\varphi} \tag{49}$$

$$\frac{\partial \Delta Q_i^{\varphi}}{\partial \theta_i^{\varphi}} = \sum_{\phi \neq \varphi} (-G_{ii}^{\varphi\phi} c_{ii}^{\varphi\phi} + B_{ii}^{\varphi\phi} s_{ii}^{\varphi\phi}) - \sum_{j:i\sim j} \sum_{\phi \in \Phi_{ij}} (-G_{ij}^{\varphi\phi} c_{ij}^{\varphi\phi} + B_{ij}^{\varphi\phi} s_{ij}^{\varphi\phi}) = -p_{i,t}^{\varphi} + G_{ii}^{\varphi\varphi} c_{ii}^{\varphi\varphi} \tag{50}$$

$$\frac{\partial \Delta Q_i^{\varphi}}{\partial |V_i^{\varphi}|} |V_i^{\varphi}| = 2B_{ii}^{\varphi\varphi} c_{ii}^{\varphi\varphi} + \sum_{\phi \neq \varphi} (G_{ii}^{\varphi\phi} s_{ii}^{\varphi\phi} + B_{ii}^{\varphi\phi} c_{ii}^{\varphi\phi}) + \sum_{j:i\sim j} \sum_{\phi \in \Phi_{ij}} (G_{ij}^{\varphi\phi} s_{ij}^{\varphi\phi} + B_{ij}^{\varphi\phi} c_{ij}^{\varphi\phi}) = -q_{i,t}^{\varphi} + B_{ii}^{\varphi\varphi} c_{ii}^{\varphi\varphi} \tag{51}$$

Therefore, the elements in the Jacobian matrix are explicitly formulated with state variables $c$ and $s$. In the next section, we will show how to replace the nonlinear constraint (23) with an LMI constraint, which can be incorporated in the general SDP-based ACOPF framework.

## III. SDP-based VSC-OPF Formulation

### A. Controlling Singular Values with SDP

Constraint (23) requires the MSV of the $\boldsymbol{J}_{PF}$ over a given value. This constraint is nonlinear and cannot be directly expressed by the state variables of the ACOPF. Different methods are designed in previous works to solve this problem [1], [23]. In general, it is nontrivial to explicitly embed the MSV of $\boldsymbol{J}_{PF}$ into the optimization framework.

In this subsection, we adopt the method to control the MSV of a matrix using SDP optimization proposed by [46]. This method is mostly used in computer graphics, and in this paper, we extend it to the power system. According to [46], the subset of matrices whose MSV is at least a constant $\lambda \geq 0$ is:

$$\mathcal{I}_{\lambda} = \left\{ \boldsymbol{A} \in \mathbb{R}^{n \times n} \middle| \sigma_{\min}(\boldsymbol{A}) \geq \lambda \right\} \tag{52}$$

$\mathcal{I}_{\lambda}$ is not convex. However, it is possible to derive its maximal convex subset using simple LMI and incorporate it in the SDP formulation. The basic formulation of the maximal convex subset of $\mathcal{I}_{\lambda}$ is:

$$\boldsymbol{C}_{\lambda} = \left\{ \boldsymbol{A} \in \mathbb{R}^{n \times n} \middle| \frac{\boldsymbol{A} + \boldsymbol{A}^{\mathrm{T}}}{2} \succcurlyeq \lambda \boldsymbol{I} \right\} \tag{53}$$

By the definition of positive semidefinite matrix, $\boldsymbol{C}_{\lambda}$ is equivalent to:

$$\boldsymbol{C}_{\lambda} = \left\{ \boldsymbol{A} \middle| \boldsymbol{x}^{\mathrm{T}} \boldsymbol{A} \boldsymbol{x} \geq \lambda, \forall \| \boldsymbol{x} \|_2 = 1, \boldsymbol{x} \in \mathbb{R}^n \right\} \tag{54}$$

To verify that it is a subset of $\mathcal{I}_{\lambda}$, let $\boldsymbol{x}$ be the unit norm eigenvector of $\boldsymbol{A}^{\mathrm{T}}\boldsymbol{A}$ corresponding to its eigenvalue $\sigma_{\min}^2(\boldsymbol{A})$, and we can obtain:

$$\| \boldsymbol{A}\boldsymbol{x} \|_2 = \sqrt{(\boldsymbol{A}\boldsymbol{x})^{\mathrm{T}} \boldsymbol{A}\boldsymbol{x}} = \sqrt{\boldsymbol{x}^{\mathrm{T}} (\sigma_{\min}^2(\boldsymbol{A}) \boldsymbol{x})} = \sigma_{\min}(\boldsymbol{A}) \| \boldsymbol{x} \|_2 \tag{55}$$

By Cauchy-Schwartz inequality, we can deduce:

$$\| \boldsymbol{A}\boldsymbol{x} \|_2 = \| \boldsymbol{x} \|_2 \| \boldsymbol{A}\boldsymbol{x} \|_2 \geq \boldsymbol{x}^{\mathrm{T}} \boldsymbol{A}\boldsymbol{x} \geq \lambda \tag{56}$$

Since $\boldsymbol{A}^{\mathrm{T}}\boldsymbol{A}$ is symmetric, $\boldsymbol{x}$ is orthogonal, $\| \boldsymbol{x} \|_2 = 1$, and we can conclude that its MSV is larger than $\lambda$:

$$\sigma_{\min}(\boldsymbol{A}) \geq \lambda \tag{57}$$

$C_{\lambda}$ is the basic formulation for the convex subset of $\mathcal{I}_{\lambda}$. So we can rewrite constraint (23) as:

$$\frac{\boldsymbol{J}_{PF,t_0}+\boldsymbol{J}_{PF,t_0}^{\mathrm{T}}}{2} \succcurlyeq \sigma_{ref}\boldsymbol{I} \tag{58}$$

It should be noted that $\boldsymbol{C}_\lambda$ does not cover the entire space of $\mathcal{I}_\lambda$, and the optimization can be performed on rotated copies of $\boldsymbol{C}_\lambda$. The rotation matrix can be obtained by polar decomposition $\boldsymbol{J}_{PF}=\boldsymbol{RS}$. The updated constraint will be:

$$\frac{\boldsymbol{R}^{\mathrm{T}}\boldsymbol{J}_{PF,t_0}+\boldsymbol{J}_{PF,t_0}^{\mathrm{T}}\boldsymbol{R}}{2} \succcurlyeq \sigma_{ref}\boldsymbol{I} \tag{59}$$

Note that the singular value of $\boldsymbol{J}_{PF}$ is an absolute proximity indicator to voltage collapse without any assumption regarding load or generator change pattern [6]. Nevertheless, the operators should be able to detect emergencies from the analysis of this value.

### *B. Finding Low-rank Solution for SDP Relaxation*

In the ACOPF, we remove the rank-1 constraint to obtain the standard SDP relaxation. If the result of (37) is a rank-1 matrix, a unique solution of $V$ can be recovered. The existence of a global optimal rank-1 solution can be proven for single-phase radial networks; however, no sufficient condition for exact relaxation in the unbalanced system exists [47]. Although numerical simulations in previous research have achieved exact results in many standard IEEE test systems, when energy storage or voltage stability constraints are considered, it cannot be guaranteed that SDP relaxation will be exact. This phenomenon is usually termed as the "rank-1 conundrum". To improve the exactness of SDP, we adopt the penalty technique from [48] to recover the low-rank solution. The original ACOPF can be reformulated as:

$$\begin{cases} \min\limits_{X}\left[f_c+\gamma\left(q_{b,t_0}+\sum\limits_{g\in\mathcal{G}}q_{g,t_0}+\sum\limits_{s\in\mathcal{S}}q_{s,t_0}\right)\right] \\ \text{s.t. (7)-(22), (32)-(36), (59)} \end{cases} \tag{60}$$

where $f_c$ is the objective function in (2); and $\gamma$ is a given positive weight. The introduction of the penalty term in the objective function aims to increase the off-diagonal entries $\boldsymbol{W}$, which, therefore, decreases the principal minors of 2-by-2 submatrices of $\boldsymbol{W}$. The effectiveness of this technique in an unbalanced distribution system can be found in [47].

The final flowchart of the proposed VSC-OPF is drawn in Fig. 2. In each optimization interval, the original VSC-OPF of (2), (7)-(22), (32)-(36) is first solved to obtain the rotation matrix $\boldsymbol{R}$. Then the VSC-OPF with the rotated VSC constraints (7)-(22), (32)-(36), (59), and (60) is solved. The result is saved for that interval and the iteration proceeds.

## IV. Case Study

In this section, case studies are carried out for the modified IEEE 13-bus, 34-bus, 37-bus, and 123-bus systems with DG, ESSs, and a non-dispatchable PV. The proposed method is first validated, and then the impact of VSC on the OPF results is studied. The optimization problem is implemented in YALMIP in MATLAB with Mosek as the SDP solver [49]. The test system data can be found in [50]. The computational tasks are performed on a personal computer with Intel Core i7 Processor (2.80 GHz) and 32 GB RAM.

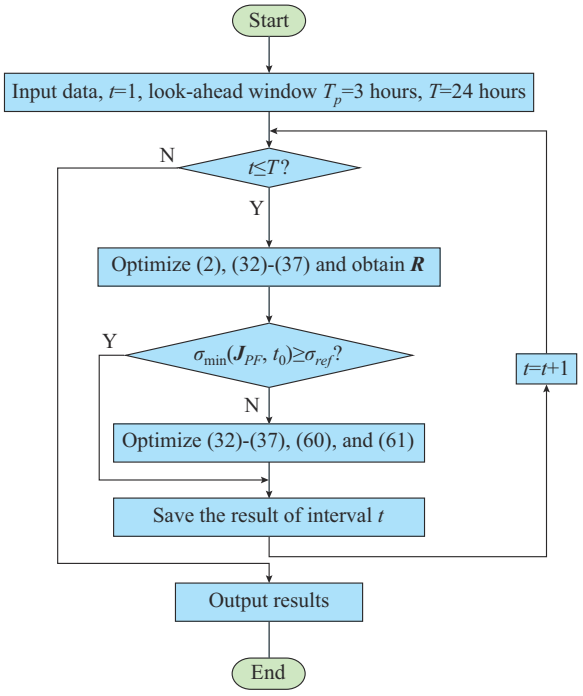


Fig. 2. Flowchart of proposed VSC-OPF.

### *A. Feasibility of Proposed Method*

We assume that the test system is connected to an upper-level main grid through bus 1 where the test system can buy power at LMP.

Bus 1 acts as the slack bus, and the other buses are all PQ buses. The proposed method models constant power loads and can be easily extended to constant impedance load as well. The operation cost is concerned with the test system, consisting of energy purchase cost from the main grid, the DG cost, and ESSs charging/discharging cost.

For validation purposes, we choose the peak-load hour and test the proposed method with a 1-hour look-ahead window. The proposed VSC-OPF method, termed "VSC", are compared with two methods.

1) "OPF": the OPF without VSC is solved as a base case.

2) "VSC": the VSC-OPF is then solved by increasing $\sigma_{ref}$ slightly over the original MSV from "OPF".

3) "ITER": an alternative iteration based VSC-OPF from [23] is adopted as a benchmark method for comparison. The inner problem of the iterative method is also solved by the SDP formulation.

The results are listed in Table I. It can be observed that the costs in VSC for all systems are higher than the base case due to the effect of MSV on operation costs. The impacts of VSC on the OPF dispatch results are investigated in detail in the following subsections. With the same MSV threshold, the proposed method can achieve smaller costs than the iterative method. However, the iterative method uses a heuristic approach to reformulate constraint (23), which encounters numerical issues in case 34 and slow convergences in all cases unless the MSV threshold is only slightly higher than the original MSV.

To evaluate the exactness of SDP relaxation, we adopt a parameter $\lambda_l$, which equals to the ratio between the second

largest and the largest eigenvalue of the matrix of (37). The average of $\lambda_l$ over all the lines is $\bar{\lambda}$, and the maximum of $\lambda_l$ of all lines is $\lambda^{\max}$. The original OPF result can be considered exact because $\lambda^{\max}$ is lower than $10^{-6}$. The proposed method is able to improve MSV while obtaining a low-rank result. The effectiveness and scalability of the proposed method are validated.

TABLE I
VALIDATION OF PROPOSED METHOD ON DIFFERENT IEEE TEST SYSTEMS

| System | Cost ($) | | | MSV | | | $\lambda^{\max}$ | | |
|---|---|---|---|---|---|---|---|---|---|
| | OPF | VSC | ITER | OPF | VSC | ITER | OPF | VSC | ITER |
| 13-bus | 13.50 | 13.51 | 13.51 | 0.560 | 0.570 | 0.570 | $1\times10^{-8}$ | $1\times10^{-9}$ | $1\times10^{-9}$ |
| 34-bus | 14.23 | 14.25 | | 0.180 | 0.190 | | $1\times10^{-6}$ | $1\times10^{-5}$ | |
| 37-bus | 3.18 | 3.19 | 3.19 | 0.344 | 0.347 | 0.347 | $1\times10^{-8}$ | $1\times10^{-8}$ | $1\times10^{-8}$ |
| 123-bus | 47.87 | 48.07 | 48.06 | 0.072 | 0.074 | 0.074 | $1\times10^{-7}$ | $1\times10^{-6}$ | $1\times10^{-6}$ |

### B. Impact of VSC on DG Dispatch

In this subsection, we investigate the impact of VSC on active/reactive power output in IEEE 13-bus and 37-bus systems. We apply the proposed method for 24 hours with a 3-hour look-ahead window. As a basic case, we run OPF without VSC and calculate the average MSV $\sigma_0$ of 24 hours. We then run additional cases where $\sigma$ indicates the percentage increase of the voltage stability margin $\sigma_{ref}$ in (60) over $\sigma_0$. The simulation results for IEEE 13-bus and 37-bus systems are given in Table II and Table III, respectively.

1) Case 1: no VSC constraint is enforced ($\sigma=0\%$).
2) Case 2: VSC-OPF is run with $\sigma=5\%$.
3) Case 3: VSC-OPF is run with $\sigma=10\%$.
4) Case 4: VSC-OPF is run with $\sigma=13\%$.

In both test systems, we start with Case 1, and obtain $\sigma_0$ in each system, and use this value multiplied by $(1+\sigma)$ as $\sigma_{ref}$ in (60) for the rest of cases.

TABLE II
SIMULATION RESULT FOR IEEE 13-BUS SYSTEM

| Case | Cost ($) | | | | $\sigma_{ref}$ | $\lambda^{\max}$ | $\bar{\lambda}$ |
|---|---|---|---|---|---|---|---|
| | Total | Main grid | DG | ESSs | | | |
| 1 | 802.64 | 500.71 | 283.15 | 18.77 | 0.5635 | $5.98\times10^{-7}$ | $6.16\times10^{-8}$ |
| 2 | 805.92 | 500.70 | 288.01 | 17.22 | 0.5927 | $1.71\times10^{-6}$ | $1.22\times10^{-7}$ |
| 3 | 827.45 | 426.40 | 392.38 | 8.67 | 0.6198 | $1.49\times10^{-5}$ | $4.42\times10^{-7}$ |
| 4 | 841.43 | 429.20 | 404.61 | 7.61 | 0.6367 | $6.97\times10^{-3}$ | $9.46\times10^{-4}$ |

TABLE III
SIMULATION RESULT FOR IEEE 37-BUS SYSTEM

| Case | Cost ($) | | | | $\sigma_{ref}$ | $\lambda^{\max}$ | $\bar{\lambda}$ |
|---|---|---|---|---|---|---|---|
| | Total | Main grid | DG | ESSs | | | |
| 1 | 512.12 | 328.46 | 169.03 | 14.74 | 0.3391 | $2.70\times10^{-6}$ | $5.66\times10^{-7}$ |
| 2 | 531.11 | 318.26 | 201.98 | 10.87 | 0.3560 | $4.08\times10^{-6}$ | $5.80\times10^{-7}$ |
| 3 | 611.35 | 373.04 | 232.17 | 5.13 | 0.3730 | $1.00\times10^{-2}$ | $1.05\times10^{-3}$ |
| 4 | 678.15 | 437.49 | 235.53 | 5.12 | 0.3832 | $2.50\times10^{-2}$ | $3.65\times10^{-3}$ |

As can be observed from Table II and Table III, increasing the VSM generally leads to higher operation cost, e.g., when $\sigma=5\%$, the total cost increases by 0.40% and 3.7% for the IEEE 13-bus and 37-bus systems, respectively; when $\sigma=13\%$, the total costs increase by 4.8% and 32% for the two systems. While the distribution of active power among different power resources is determined by the configuration of the individual system, it is clear that for both systems, after the introduction of VSC, ESS costs are reduced and DG costs are increased. To investigate the effect of VSC on the power dispatch, we plot the active and reactive power exchange with the main grid, DG outputs, as well as the ESS charging/discharging in Fig. 3 and Fig. 4 regarding different cases.

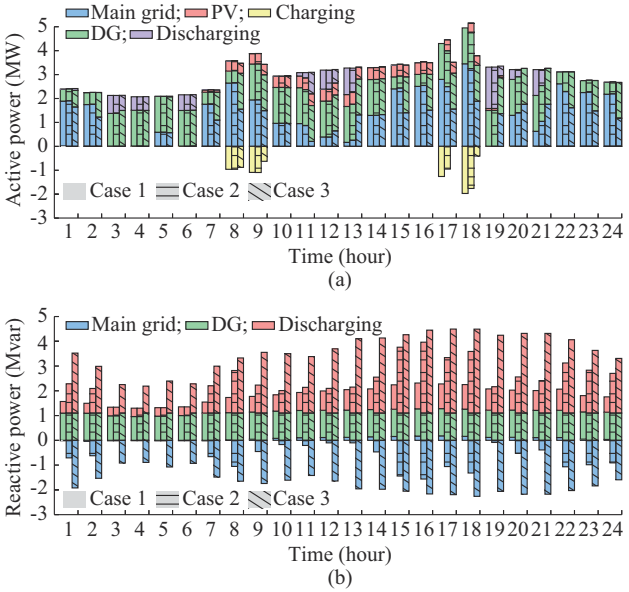


Fig. 3. Dispatch result of IEEE 13-bus system. (a) Active power. (b) Reactive power.

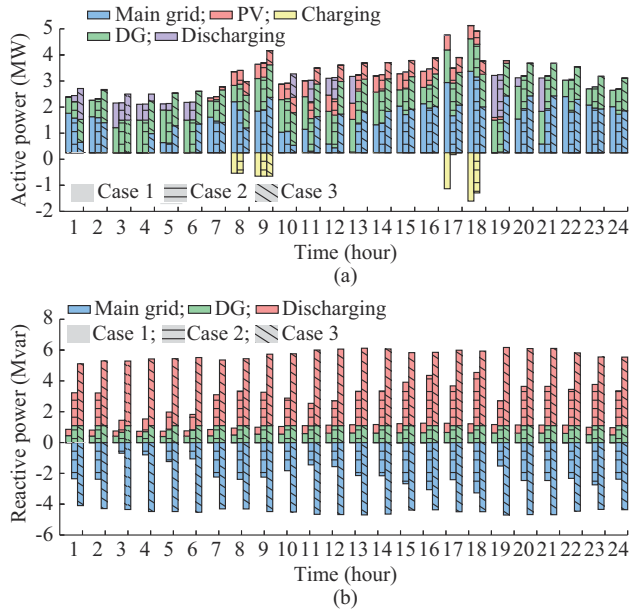


Fig. 4. Dispatch result of IEEE 37-bus system. (a) Active power. (b) Reactive power.

It is evident that the increased voltage stability margin can influence both the active and reactive power dispatches. In particular, ESSs can harness the volatility of the LMP throughout the day for energy arbitrage. However, as charging ESSs act as a load, higher charging power will negatively impact the voltage stability level. As $\sigma$ increases, the charging power of ESSs drops, and the reactive power discharged from ESSs increases. The VSC constraint will also change the voltage profile. Figure 5 shows the voltage amplitude of the IEEE 13-bus and 123-bus systems at the 18th hour. As $\sigma$ increases, the voltage profile of the 13-bus system is improved accordingly. The voltage profile of the IEEE 123-bus system shows that the mean voltage amplitude over all buses is improved by VSC but not all bus voltage amplitudes are increased. The average voltage amplitude can be obtained through the matrix $\boldsymbol{u}_i$. Suppose that for bus $i$, $\Phi_i=\{a,b,c\}$, then the diagonal elements of $u_i$ correspond to:

$$\mathrm{diag}(\boldsymbol{u}_i)=\left[|V_i^a|^2,|V_i^b|^2,|V_i^c|^2\right] \tag{62}$$

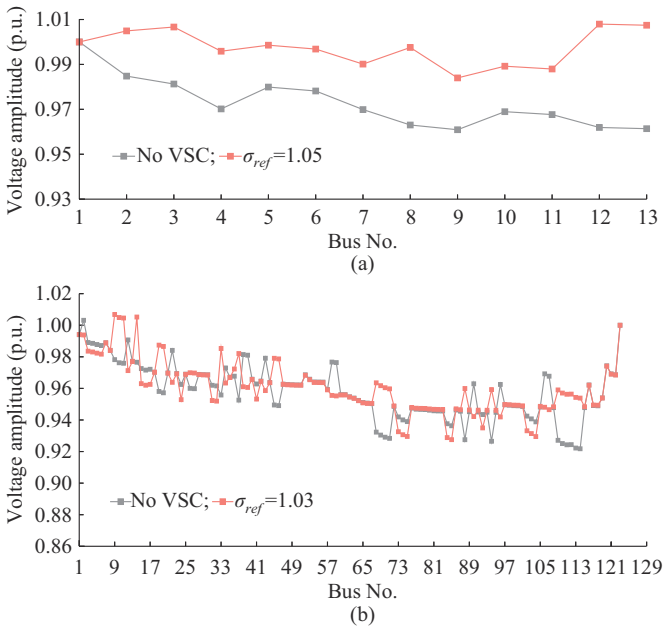


Fig. 5. Voltage amplitude of IEEE 13-bus and 123-bus systems at the 18th hour. (a) IEEE 13-bus system. (b) IEEE 123-bus system.

The voltage amplitude of phase $\varphi$ is:

$$|V_i^{\varphi}|=\sqrt{|V_i^{\varphi}|^2} \tag{63}$$

Here we take the average of the voltage amplitude over the cardinality of $\Phi_i$ to show the average voltage profile:

$$|\bar{V}_i|=\sum_{\varphi\in\Phi_i}\frac{|V_i^{\varphi}|}{|\Phi_i|} \tag{64}$$

For the reactive power, we can observe that the increase of VSC leads to a significant change in the pattern of the reactive power dispatch. As $\sigma$ increases, the reactive power from the ESS increases, and the main grid also absorbs more reactive power.

For all cases, as the VSC is increased by $\sigma$, the second largest eigenvalue is still significantly smaller than the largest eigenvalue, so the SDP can be considered approximately exact or at least low-rank. However, the exactness of the SDP relaxation is reduced as the voltage stability margin is increased.

### C. Influence of Load Variation on VSM

In this subsection, we investigate the effect of load levels on the results of the IEEE 13-bus system. Figure 5 gives the hourly load profile for one day and the corresponding hourly MSV from case 1 to case 4. When there is no VSC constraint, it can be observed that the trend of MSV in case 1 is inversely proportional to the load level. In general, a higher load level usually means a lower MSV, and vice versa. For hours 3-6, the MSV of the original OPF result already satisfies the requirement of $\sigma=5\%$, and the costs of two systems coincide for that period in Fig. 6(b). This demonstrates that VSC-OPF can be performed only at peak load hours when the VSM is small, and the risk of voltage instability is high. When $\sigma=10\%$, the MSV throughout the day is increased, and the hourly cost is also higher than the cost of the system with no VSC or a lower $\sigma$.

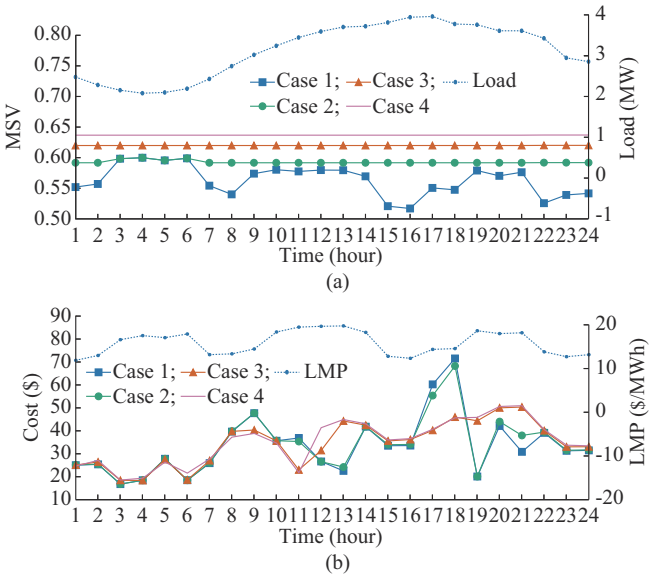


Fig. 6. Hourly MSV and cost of IEEE 13-bus system. (a) Hourly MSV and load. (b) Hourly cost and LMP.

The system cost is also influenced by the LMP from the main grid, which is the blue dashed line in Fig. 6(b). The three-hour look ahead window allows ESSs to detect LMP fluctuation, and ESSs will be charged at a lower LMP and discharge later. As shown in the previous subsection, when VSC is employed, the charging power of ESSs is reduced. This trend is also reflected in the hourly cost plot. The system without VSC will have higher costs during low-LMP periods due to ESSs charging and lower costs later. As $\sigma$ increases, the overall costs increase, while the costs at lower LMPs drop because the charging cost of ESSs is reduced.

### D. Influence of ESSs on VSM

As shown in the previous subsection, ESSs can achieve energy arbitrage. However, VSC may limit the active charg-

ing power of ESSs. Thus, when VSC is considered, the energy charged by the ESSs is reduced. However, another important function of ESSs is to provide reactive power support to the system. We rerun the VSC-OPF for test systems without ESSs, and the results are shown in Tables IV and V. The average MSV values in case 1 for the two systems are 0.5510 and 0.3380, respectively, less than those with ESSs. This demonstrates that even without VSC, the existence of ESSs can help improve the overall VSM. The hourly cost and reactive power dispatch for the IEEE 37-bus system without ESSs are plotted in Fig. 7. There is a clear trend that higher VSM leads to higher costs. Without reactive power support from ESSs, the main-grid has to provide reactive power from the 11th hour to 22nd hour.

TABLE IV
COST FOR IEEE 13-BUS SYSTEM WITHOUT ESSS

| Case | Cost ($) | | | $\sigma_{ref}$ |
|---|---|---|---|---|
| | Total | Main grid | DG | |
| 1 | 845.62 | 563.59 | 282.03 | 0.5510 |
| 2 | 859.52 | 484.54 | 374.98 | 0.5806 |
| 3 | 880.64 | 469.27 | 411.37 | 0.6061 |

TABLE V
COST FOR IEEE 37-BUS SYSTEM WITHOUT ESSS

| Case | Cost ($) | | | $\sigma_{ref}$ |
|---|---|---|---|---|
| | Total | Main grid | DG | |
| 1 | 550.72 | 382.26 | 168.46 | 0.3380 |
| 2 | 567.81 | 343.07 | 224.73 | 0.3465 |
| 3 | 676.48 | 436.48 | 239.99 | 0.3630 |

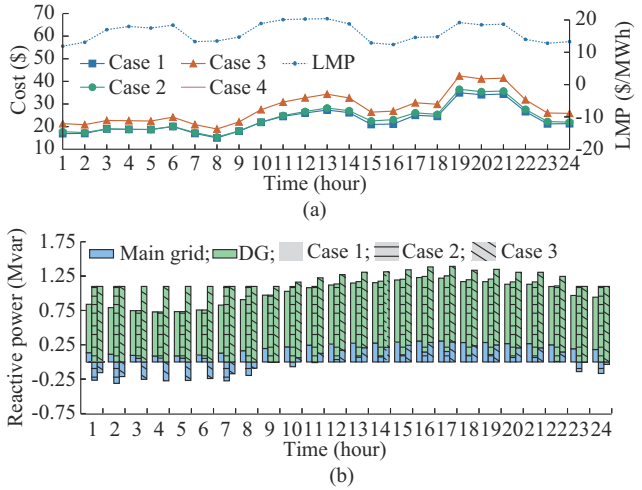


Fig. 7. Hourly cost and reactive power dispatch for IEEE 37-bus system without ESSs. (a) Hourly cost. (b) Reactive power dispatch.

### E. Influence of Unbalanced Operation on VSM

One of the characteristics of the power distribution system is its unbalanced operation. In this subsection, we set up three cases of different balanced levels for comparison.

1) "Original": IEEE 13-bus case 1 from Section IV-B.

2) "Balanced": based on the "Original", the loads are evenly redistributed among the phases.

3) "More unbalanced": based on "Original", the load is redistributed more unevenly.

Figure 8 shows that different levels of unbalance lead to different VSM. Throughout the day, the hourly MSV indicates that a more balanced system will have a higher VSM, e.g., at the 17th hour, the MSV of a balanced case is 2.02% higher than that of the unbalanced case. The VSM difference is more prominent in peak load hours. When the load is low, it can be observed that the three cases achieve almost the same MSV. Table VI shows the cost comparison with different balanced levels. We can observe that the cost of the more unbalanced case is higher than the original case and the balanced case. These observations also emphasize the importance of considering unbalanced operation in VSC-OPF.

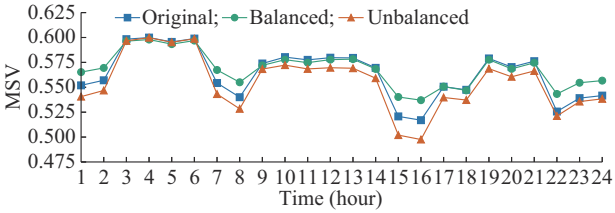


Fig. 8. MSV of systems with different unbalanced level.

TABLE VI
COST COMPARISON WITH DIFFERENT UNBALANCED LEVELS

| Unbalanced level | Cost ($) | | | | $\sigma_{ref}$ |
|---|---|---|---|---|---|
| | Total | Main grid | DG | ESS | |
| Balanced, no VSC | 801.57 | 499.65 | 283.14 | 18.78 | 0.5700 |
| Balanced, $\sigma$=5% | 812.28 | 451.29 | 350.28 | 10.74 | 0.5986 |
| Unbalanced, no VSC | 803.58 | 501.42 | 283.37 | 18.78 | 0.5537 |
| Unbalanced, $\sigma$=5% | 813.29 | 434.44 | 366.50 | 12.33 | 0.5840 |

## V. CONCLUSION

A novel method to incorporate voltage stability constraints in the unbalanced distribution system OPF problem is proposed in this paper. The MSV of the power flow Jacobian matrix is taken as a metric for voltage stability. The constraint on the MSV is reformulated as an LMI and can be incorporated in the SDP-based ACOPF model. This reformulation allows the algorithm to find the optimal solution in the maximal convex subset of the original voltage stability constraints. The case studies validate the proposed method. Simulation results show that the proposed method can effectively improve the VSM of the test systems, and the effect of VSC on operation costs and power dispatch results are presented. A penalty technique is employed to achieve a low-rank OPF solution. While most of the VSC-OPF solutions remain low-rank, as the VSM increases, the exactness of the SDP-OPF is gradually decreased. The future research direction is to find better methods to improve the SDP relaxation exactness and the evaluation of the proper MSV threshold. New methods with less computation burdens are desired to consider stochastic scenarios in power system operation.

## REFERENCES


[1] C. Wang, B. Cui, Z. Wang *et al.*, "SDP-based optimal power flow with steady-state voltage stability constraints," *IEEE Transactions on Smart Grid*, vol. 10, no. 4, pp. 4637-4647, Jul. 2018.

[2] Z. Tang, X. Li, S. Dusmez *et al.*, "A new V/f-based sensorless MTPA control for IPMSM drives," *IEEE Transactions on Power Electronics*, vol. 31, no. 6, pp. 4400-4415, Jun. 2015.

[3] X.-P. Zhang, P. Ju, and E. Handschin, "Continuation three-phase power flow: a tool for voltage stability analysis of unbalanced three-phase power systems," *IEEE Transactions on Power Systems*, vol. 20, no. 3, pp. 1320-1329, Aug. 2005.

[4] P. Kundur, N. J. Balu, and M. G. Lauby, *Power System Stability and Control*. New York: McGraw-Hill, 1994.

[5] B. Cui and X. Sun, "A new voltage stability-constrained optimal power-flow model: sufficient condition, SOCP representation, and relaxation," *IEEE Transactions on Power Systems*, vol. 33, no. 5, pp. 5092-5102, Sept. 2018.

[6] C. Cañizares, W. Rosehart, A. Berizzi *et al.*, "Comparison of voltage security constrained optimal power flow techniques," in *Proceedings of 2001 Power Engineering Society Summer Meeting*, Vancouver, Canada, Jul. 2001, pp. 1680-1685.

[7] A. Jalali and M. Aldeen, "Risk-based stochastic allocation of ESS to ensure voltage stability margin for distribution systems," *IEEE Transactions on Power Systems*, vol. 34, no. 2, pp. 1264-1277, Mar. 2018.

[8] A. Rabiee, S. Nikkhah, and A. Soroudi, "Information gap decision theory to deal with long-term wind energy planning considering voltage stability," *Energy*, vol. 147, pp. 451-463, Mar. 2018.

[9] R. Zafar, J. Ravishankar, J. E. Fletcher *et al.*, "Multi-timescale voltage stability-constrained volt/var optimization with battery storage system in distribution grids," *IEEE Transactions on Sustainable Energy*, vol. 11, no. 2, pp. 868-878, Apr. 2020.

[10] M. Jadidbonab, M. Vahid-Pakdel, H. Seyedi *et al.*, "Stochastic assessment and enhancement of voltage stability in multi carrier energy systems considering wind power," *International Journal of Electrical Power & Energy Systems*, vol. 106, pp. 572-584, Mar. 2019.

[11] J. Modarresi, E. Gholipour, and A. Khodabakhshian, "A comprehensive review of the voltage stability indices," *Renewable and Sustainable Energy Reviews*, vol. 63, pp. 1-12, Sept. 2016.

[12] M. Kashem, V. Ganapathy, and G. Jasmon, "Network reconfiguration for enhancement of voltage stability in distribution networks," *IEE Proceedings – Generation, Transmission and Distribution*, vol. 147, pp. 171-175, May 2000.

[13] C. Zheng and M. Kezunovic, "Distribution system voltage stability analysis with wind farms integration," in *Proceedings of North American Power Symposium 2010*, Arlington, USA, Sept. 2010, pp. 1-6.

[14] A. A. Mohamed and B. Venkatesh, "Line-wise power flow and voltage collapse," *IEEE Transactions on Power Systems*, vol. 33, no. 4, pp. 3768-3778, Dec. 2017.

[15] A. A. Mohamed and B. Venkatesh, "Voltage stability constrained line-wise optimal power flow," *IET Generation, Transmission & Distribution*, vol. 13, pp. 1332-1338, Apr. 2019.

[16] M.-A. Nasr, S. Nikkhah, G. B. Gharehpetian *et al.*, "A multi-objective voltage stability constrained energy management system for isolated microgrids," *International Journal of Electrical Power & Energy Systems*, vol. 117, p. 105646, May 2020.

[17] Y. Mansour, W. Xu, F. Alvarado *et al.*, "SVC placement using critical modes of voltage instability," *IEEE Transactions on Power Systems*, vol. 9, no. 2, pp. 757-763, May 1994.

[18] Z. Wang, B. Cui, and J. Wang, "A necessary condition for power flow insolvability in power distribution systems with distributed generators," *IEEE Transactions on Power Systems*, vol. 32, no. 2, pp. 1440-1450, Mar. 2016.

[19] L. Aolaritei, S. Bolognani, and F. Dörfler, "Hierarchical and distributed monitoring of voltage stability in distribution networks," *IEEE Transactions on Power Systems*, vol. 33, no. 6, pp. 6705-6714, Jun. 2018.

[20] P.-A. Lof, T. Smed, G. Andersson *et al.*, "Fast calculation of a voltage stability index," *IEEE Transactions on Power Systems*, vol. 7, no. 1, pp. 54-64, Feb. 1992.

[21] A. Tiranuchit and R. Thomas, "A posturing strategy against voltage instabilities in electric power systems," *IEEE Transactions on Power Systems*, vol. 3, no. 1, pp. 87-93, Feb. 1988.

[22] S. Raj and B. Bhattacharyya, "Weak bus-oriented optimal var planning based on grey wolf optimization," in *Proceedings of 2016 National Power Systems Conference (NPSC)*, Bhubaneswar, India, Dec. 2016, pp. 1-5.

[23] R. J. Avalos, C. A. Canizares, and M. F. Anjos, "A practical voltage-stability-constrained optimal power flow," in *Proceedings of 2008 IEEE Power and Energy Society General Meeting – Conversion and Delivery of Electrical Energy in the 21st Century*, Pittsburgh, USA, Jul. 2008, pp. 1-6.

[24] S. K. Kodsi and C. A. Canizares, "Application of a stability-constrained optimal power flow to tuning of oscillation controls in competitive electricity markets," *IEEE Transactions on Power Systems*, vol. 22, no. 4, pp. 1944-1954, Nov. 2007.

[25] M. Yao, D. K. Molzahn, and J. L. Mathieu, "An optimal power-flow approach to improve power system voltage stability using demand response," *IEEE Transactions on Control of Network Systems*, vol. 6, no. 3, pp. 1015-1025, Sept. 2019.

[26] S. Abhyankar, G. Geng, M. Anitescu *et al.*, "Solution techniques for transient stability-constrained optimal power flow – part I," *IET Generation, Transmission & Distribution*, vol. 11, pp. 3177-3185, Aug. 2017.

[27] G. Geng, V. Ajjarapu, and Q. Jiang, "A hybrid dynamic optimization approach for stability constrained optimal power flow," *IEEE Transactions on Power Systems*, vol. 29, no. 5, pp. 2138-2149, Sept. 2014.

[28] M. Paramasivam, A. Salloum, V. Ajjarapu *et al.*, "Dynamic optimization based reactive power planning to mitigate slow voltage recovery and short term voltage instability," *IEEE Transactions on Power Systems*, vol. 28, no. 4, pp. 3865-3873, Nov. 2013.

[29] C. Ye and M. Huang, "Multi-objective optimal power flow considering transient stability based on parallel NSGA-II," *IEEE Transactions on Power Systems*, vol. 30, no. 2, pp. 857-866, Mar. 2015.

[30] O. Rattananatthaworn, "Transient stability constrained optimal power flow by particle swarm optimization with time varying acceleration coefficients," in *Proceedings of 2019 IEEE PES GTD Grand International Conference and Exposition Asia*, Bangkok, Thailand, Mar. 2019, pp. 774-778.

[31] P. Kayal and C. Chanda, "Placement of wind and solar based DGS in distribution system for power loss minimization and voltage stability improvement," *International Journal of Electrical Power & Energy Systems*, vol. 53, pp. 795-809, Dec. 2013.

[32] J. Liu, Y. Xu, Z. Dong *et al.*, "Retirement-driven dynamic var planning for voltage stability enhancement of power systems with high-level wind power," *IEEE Transactions on Power Systems*, vol. 33, no. 2, pp. 2282-2291, Mar. 2017.

[33] Y. Zhou, Q. Guo, H. Sun *et al.*, "A novel data-driven approach for transient stability prediction of power systems considering the operational variability," *International Journal of Electrical Power & Energy Systems*, vol. 107, pp. 379-394, May 2019.

[34] Z. Shi, W. Yao, L. Zeng *et al.*, "Convolutional neural network-based power system transient stability assessment and instability mode prediction," *Applied Energy*, vol. 263, p. 114586, Apr. 2020.

[35] S. Li, J. Hou, A. Yang *et al.*, "DNN-based distributed voltage stability online monitoring method for large-scale power grids," *Frontiers in Energy Research*, vol. 9, pp. 1-8, Mar. 2021.

[36] K. D. Dharmapala, A. Rajapakse, K. Narendra *et al.*, "Machine learning based real-time monitoring of long-term voltage stability using voltage stability indices," *IEEE Access*, vol. 8, pp. 222544-222555, Dec. 2020.

[37] M. Ettehadi, H. Ghasemi, and S. Vaez-Zadeh, "Voltage stability-based dg placement in distribution networks," *IEEE Transactions on Power Delivery*, vol. 28, no. 1, pp. 171-178, Oct. 2013.

[38] R. S. A. Abri, E. F. El-Saadany, and Y. M. Atwa, "Optimal placement and sizing method to improve the voltage stability margin in a distribution system using distributed generation," *IEEE Transactions on Power Systems*, vol. 28, no. 1, pp. 326-334, Feb. 2013.

[39] C. Wang, B. Cui, and Z. Wang, "Analysis of solvability boundary for droop-controlled microgrids," *IEEE Transactions on Power Systems*, vol. 33, no. 5, pp. 5799-5802, Sept. 2018.

[40] S. D. Beigvand, H. Abdi, and S. N. Singh, "Voltage stability analysis in radial smart distribution grids," *IET Generation, Transmission & Distribution*, vol. 11, pp. 3722-3730, May 2017.

[41] G. Carpinelli, D. Lauria, and P. Varilone, "Voltage stability analysis in unbalanced power systems by optimal power flow," *IEE Proceedings – Generation, Transmission and Distribution*, vol. 153, pp. 261-268, May 2006.

[42] G. Carpinelli, P. Caramia, A. Russo *et al.*, "Voltage stability in unbalanced power systems: a new complementarity constraints-based approach," *IET Generation, Transmission & Distribution*, vol. 9, pp. 2014-2023, Oct. 2015.

[43] L. Gan and S. H. Low, "Convex relaxations and linear approximation for optimal power flow in multiphase radial networks," in *Proceedings*

*of 2014 Power Systems Computation Conference*, Wroclaw, Poland, Aug. 2014, pp. 1-9.
[44] Y. Liu, J. Li, L. Wu *et al.*, "Chordal relaxation based ACOPF for unbalanced distribution systems with DERs and voltage regulation devices," *IEEE Transactions on Power Systems*, vol. 33, no. 1, pp. 970-984, Jan. 2017.
[45] D. K. Molzahn and I. A. Hiskens, "A survey of relaxations and approximations of the power flow equations," *Foundations and Trends in Electric Energy Systems*, vol. 4, no. 102, pp. 1-221, Feb. 2019.
[46] S. Z. Kovalsky, N. Aigerman, R. Basri *et al.*, "Controlling singular values with semidefinite programming," *ACM Transactions on Graphics (TOG)*, vol. 33, no. 4, pp. 1-13, Jul. 2014.
[47] W. Wang and N. Yu, "Chordal conversion based convex iteration algorithm for three-phase optimal power flow problems," *IEEE Transactions on Power Systems*, vol. 33, no. 2, pp. 1603-1613, Mar. 2017.
[48] R. Madani, S. Sojoudi, and J. Lavaei, "Convex relaxation for optimal power flow problem: mesh networks," *IEEE Transactions on Power Systems*, vol. 30, no. 1, pp. 199-211, Jan. 2015.
[49] J. Löfberg, "YALMIP: a toolbox for modeling and optimization in MATLAB," in *Proceedings of the 2004 IEEE International Conference on Robotics and Automation*, Taipei, China, Sept. 2004, pp. 1-6.
[50] Personal site of Yanling Lin. (2021, Apr.). Distribution system. [Online]. Available: https://sites. google. com/view/yanlinglin/data/distribution-system

**Yanling Lin** received the B.S. degree in electrical engineering from Shandong University, Jinan, China, in 2013, and the Ph.D. degree at Xi'an Jiaotong University, Xi'an, China, in 2019. She is currently working toward the Ph.D. degree in Southern Methodist University, Dallas, USA. Her research interests include power system resilience, energy market, and renewable energy integration.

**Xiaohu Zhang** received the B.S. degree in electrical engineering from Huazhong University of Science and Technology, Wuhan, China, in 2009, the M.S. degree in electrical engineering from the Royal Institute of Technology, Stockholm, Sweden, in 2011, and the Ph.D. degree in electrical engineering from the University of Tennessee, Knoxville, USA, in 2017. His research interests include power system operation, planning and stability analysis.

**Jianhui Wang** is a Professor with the Department of Electrical and Computer Engineering at Southern Methodist University, Dallas, USA. He has authored and/or co-authored more than 300 journal and conference publications, which have been cited for more than 30000 times by his peers with an H-index of 93. He has been invited to give tutorials and keynote speeches at major conferences including IEEE ISGT, IEEE SmartGridComm, IEEE SEGE, IEEE HPSC and IGEC-XI. He is the past Editor-in-Chief of the IEEE Transactions on Smart Grid and an IEEE PES Distinguished Lecturer. He is also a Guest Editor of a Proceedings of the IEEE special issue on power grid resilience. He is the Recipient of the IEEE PES Power System Operation Committee Prize Paper Award in 2015, the 2018 Premium Award for Best Paper in IET Cyber-Physical Systems: Theory & Applications, and the Best Paper Award in IEEE Transactions on Power Systems in 2020. He is a Clarivate Analytics highly cited researcher for production of multiple highly cited papers that rank in the top 1% by citations for field and year in Web of Science (2018-2021). He is a Fellow of IEEE. His research interests include smart grid, microgrid, cybersecurity, grid resilience, renewable integration, energy economics and policy, electric power systems operations and control, electricity restructuring.

**Di Shi** received the Ph. D. degree in electrical engineering from Arizona State University, Tempe, USA, in 2012. He is the Founder of AINERGY LLC, Santa Clara, USA. He was the Director of Fundamental R&D Center and Department Head of AI & System Analytics, GEIRINA, San Jose, USA, and a Research Staff Member with NEC Laboratories America, Princeton, USA. He is the Editor of the IEEE Transactions on Smart Grid and the IEEE Power Engineering Letters. His research interests include data analytics, energy storage systems, and applications of artificial intelligence and Internet of Things in power systems.

**Desong Bian** received the M.S. degree from University of Florida, Gainesville, USA, in 2012, and the Ph.D. degree from Virginia Tech, Blacksburg, USA, in 2016. His research interests include implementation of renewable energy, smart energy management system, and application of machine learning in smart grid.